HHS Public Access

Author manuscript

*Biochim Biophys Acta*. Author manuscript; available in PMC 2016 January 01.

Published in final edited form as:

*Biochim Biophys Acta*. 2015 January ; 1848(1 0 0): 334–341. doi:10.1016/j.bbamem.2014.05.003.

# Correlating Lipid Bilayer Fluidity with Sensitivity and Resolution of Polytopic Membrane Protein Spectra by Solid-State NMR Spectroscopy

**James R. Banigan**, **Anindita Gayen**, and **Nathaniel J Traaseth**

Department of Chemistry, New York University, New York, NY 10003

## Abstract

Solid-state NMR spectroscopy has emerged as an excellent tool to study the structure and dynamics of membrane proteins under native-like conditions in lipid bilayers. One of the key considerations in experimental design is the uniaxial rotational diffusion of the protein that can have a direct influence on the NMR spectral observables. In this regard, temperature plays a fundamental role in modulating the phase properties of the lipids, which directly influences the rotational diffusion rate of the protein in the bilayer. In fact, it is well established that below the main phase transition temperature of the lipid bilayer the protein's motion is significantly slowed while above this critical temperature the rate is increased. In this article, we carried out a systematic comparison of the signal intensity and spectral resolution as a function of temperature using magic-angle-spinning (MAS) solid-state NMR spectroscopy. These observables were directly correlated with the relative fluidity of the lipid bilayer as inferred from differential scanning calorimetry (DSC). We applied our hybrid biophysical approach to polytopic membrane protein multidrug resistance transporters (EmrE and SugE) in the presence of model membrane lipid compositions (DMPC-14:0 and DPPC-16:0). From these experiments, we conclude that the rotational diffusion giving optimal spectral resolution corresponds to a bilayer fluidity of ~5%, which corresponds to the percentage of lipids in the fluid or liquid-crystalline fraction. At the temperature corresponding to this *critical value of fluidity*, there is sufficient mobility to reduce inhomogeneous line broadening that occurs at lower temperatures. A greater extent of fluidity leads to faster uniaxial rotational diffusion and a sigmoidal-type drop in the NMR signal intensity, which stems from intermediate-exchange dynamics where the motion has a similar frequency as the NMR observables (i.e., dipolar couplings and chemical shift anisotropy). These experiments provide insight into the optimal temperature ranges and corresponding bilayer fluidity to study membrane proteins by solid-state NMR spectroscopy.

## Graphical abstract



CORRESPONDING AUTHOR FOOTNOTE: Department of Chemistry, New York University, 100 Washington Square East, New York, NY 10003, traaseth@nyu.edu.

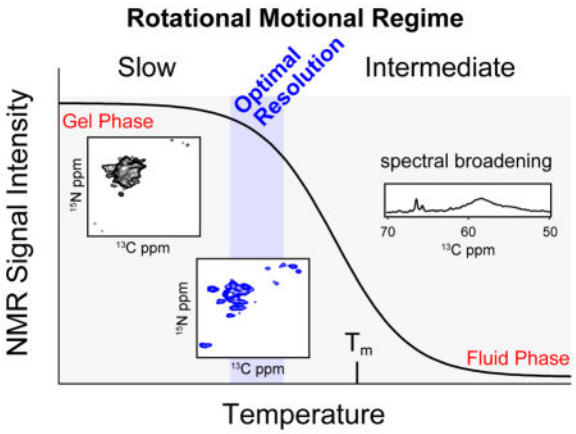


**Keywords**

Membrane proteins; membrane composition; bilayer fluidity; differential scanning calorimetry; solid-state NMR; EmrE; small multidrug resistance family; multidrug resistance

## INTRODUCTION

Membrane protein structure determination is important for deciphering molecular-scale details of essential biological events including ion homeostasis, cell signaling pathways, and transport of metabolites. Both NMR and X-ray crystallography have contributed to the knowledge database of the structures for these hydrophobic proteins. One method that has gained traction in recent years is solid-state NMR spectroscopy. In this technique, it is possible to study the proteins under native-like conditions such as phospholipid bilayers that are better mimics to cellular membranes than detergent micelles. Indeed, synthetic lipid membranes have been extensively studied and are often used for reconstituting membrane proteins for solid-state NMR and EPR spectroscopy [1–6]. The two major disciplines within solid-state NMR for characterizing membrane proteins are magic-angle-spinning (MAS) [7–10] and the oriented approach [11–13]. The latter has been extensively used to probe the tilt angles of membrane protein secondary structures with respect to the lipid bilayer as well as for backbone structure determination [1, 14–22]. The MAS method is more commonly employed due to the simplified sample preparations that do not require the protein to be macroscopically aligned in the magnetic field. In addition, it is common to obtain one or more $^{13}$C detection periods such as the *afterglow* method [23, 24] that substantially enhances sensitivity over $^{15}$N detection schemes commonly employed in oriented approaches. For both methods, one of the intrinsic motional parameters that affects the ability to record high-quality structural data is the presence of uniaxial rotational motion about the membrane normal [25–28]. Indeed, when this diffusion rate is comparable to the frequency of the NMR observables, signal-to-noise and resolution suffer [29] and the spectra become difficult to interpret. Unlike microcrystalline soluble and membrane proteins studied by MAS, these intrinsic motional properties also depend on the fluidity of the membrane. In model lipid membrane compositions, the two relevant phase regions below the melting temperature ($T_m$) correspond to the gel and ripple phases [30, 31]. For synthetic

phospholipid bilayers, the primary parameter that dictates the largest fluidity of the membrane is the main phase transition [32]. Above $T_m$, the lipids are in the liquid-crystalline state, in which the hydrocarbon chains are in a disordered, fluid-like state [30]. Indeed, it has been documented that below the main phase transition, the uniaxial rotational diffusion is significantly slowed while above the $T_m$, the diffusional rate is increased in the fluid phase of the lipid bilayer [33]. The ripple phase or pre-transition corresponds with the beginning of bilayer melting, in which some of the lipids are in a semi-ordered, gel-like phase interspersed with lipids in the more fluid and disordered liquid-crystalline phase [34, 35]. Below the pre-transition, the bilayer is in a solid-like gel phase. The incorporation of membrane proteins into the lipid bilayer results in a broadening of both the pre-transition and main phase transition such that at relatively low lipid:protein ratios the former can be broad beyond detection [36–38].

In this work, we took a systematic approach to correlating the membrane fluidity with the solid-state NMR spectral quality from MAS (sensitivity and resolution) for polytopic membrane transporters from the small multidrug resistant (SMR) family. Our experiments involved measuring main phase transitions of proteoliposomes (SMR proteins in DMPC and DPPC) using differential scanning calorimetry (DSC) and acquisition of multidimensional MAS spectra under a wide range of temperatures. Our findings serve as a guide for optimizing membrane protein studies by MAS and show that the optimal rotational dynamics for high quality NMR spectra of polytopic membrane proteins requires diffusional rates that are neither too fast nor too slow.

## 2. METHODS

### 2.1 Growth and Purification of EmrE and SugE

EmrE was expressed as a fusion protein with maltose binding protein (MBP) in BL21 (DE3) cells. To selectively incorporate [2-$^{13}$C,$^{15}$N] Leu, cells were grown in M9 minimal media containing 120 mg/L of [2-$^{13}$C,$^{15}$N] Leu (Sigma-Aldrich), 800 mg/L of natural abundance Ile and Val, and 300 mg/L of all other amino acids. For simultaneous incorporation of Leu and Val, the media contained 120 mg/L of [2-$^{13}$C,$^{15}$N] Leu, 120 mg/L of [$^{13}C_5$,$^{15}$N] Val (Sigma-Aldrich), 800 mg/L of natural abundance Ile, and 300 mg/L of all other amino acids. EmrE was purified as previously described [1, 24]. Reverse-IL labeled SugE (U-[$^{13}$C,$^{15}$N] with natural abundance Ile and Leu) was grown and purified in the same manner as EmrE [24].

### 2.2 Reconstitution of EmrE into DPPC or DMPC Liposomes

EmrE was purified in DDM detergent (buffer: 20 mM $Na_2HPO_4$ and 20 mM NaCl at pH 6.9) and reconstituted into 1,2-dimyristoyl-sn-glycero-3-phosphocholine (DMPC) or 1,2-dipalmitoyl-sn-glycero-3-phosphocholine (DPPC) (Avanti Polar Lipids) using Bio-Beads (Biorad) overnight at 4 °C (45:1 w:w of Bio-Beads to detergent). Proteoliposomes were pelleted via ultracentrifugation at 177,000 x g (max) for 1.5 hours. For NMR samples, the buffer was exchanged to 20 mM HEPES (pH 6.9), 20 mM NaCl, 50 mM DTT, and 0.05% $NaN_3$ and packed into the 3.2 mm MAS rotor.

### 2.3 Differential Scanning Calorimetry

DSC experiments were performed with a nanoDSC (model 6300; TA Instruments). The samples were suspended in 20 mM $Na_2HPO_4$, 20 mM NaCl at pH 6.9. The apo EmrE experiments used a lipid:monomer ratio of 100:1 (mol:mol). The lipid concentration in the experiments was 9.2 mM. The temperature range for DSC was 4–55 °C with a scanning rate of 4.8 °C/hr at a constant pressure of 3 atm and 600 sec of equilibration time prior to scanning. A blank run was performed with buffer alone and subtracted from the sample curves to obtain $\Delta C_p$. Data was analyzed using NanoAnalyze v2.4.1 (TA Instruments), Gnuplot v4.6, and Matlab vR2012a (MathWorks).

### 2.4 NMR Spectroscopy

The pelleted proteoliposomes were partially dehydrated using lyophilization and then center-packed into 3.2 mm thin-walled rotors using sample spacers. All MAS experiments were performed at 14.1 T using a DD2 spectrometer (Agilent) with a BioMAS probe (Agilent) doubly tuned to $^{1}H$ and $^{13}C$ or triply tuned to $^{1}H$, $^{13}C$, and $^{15}N$. The 90° pulses for $^{1}H$, $^{13}C$, and $^{15}N$ corresponded to frequency strengths $\omega/2\pi$ of 100 kHz, 45.5 kHz, and 45.5 kHz, respectively. MAS rates were 10 kHz or 12.5 kHz. The temperature titration 1D $^{1}H$-$^{13}C$ cross-polarization experiments used a contact time of 200 μs, an acquisition time of 25 msec, a $^{13}C$ spectral width of 100 kHz, and TPPM $^{1}H$ decoupling [39] at 100 kHz ($\omega/2\pi$). 2D NCA experiments were acquired on $TPP^{+}$ bound [2-$^{13}C$,$^{15}N$-Leu]-EmrE in DMPC. The $^{1}H$-$^{15}N$ contact time was 600 μsec or 950 μsec (shorter at warmer temperatures to compensate for $^{1}H$ $T_{1\rho}$ values). The transfer from $^{15}N$ to $^{13}CA$ used SPECIFIC-CP [40] and a contact time of 3.5 to 4.5 msec (shorter at warmer temperatures). The indirect dimension had a spectral width of 3125 Hz and 8 msec of acquisition. The direct dimension had a spectral width of 100 kHz and 25 msec of acquisition time. The 2D spectra were acquired with 64 scans (−21 °C, −10 °C, −1 °C), 128 scans (9 °C), or 320 scans (14 °C) to partially account for the loss in signal-to-noise from increases in temperature. The variable temperature display and effect of spinning was calibrated using methanol [41]. The heating due to decoupling was determined with KBr inside a rotor containing DMPC hydrated with the buffer, to simulate a protein sample. Specifically, KBr (~16.5 mg) was placed between the top spacer and the rotor cap and did not mix with the lipid. The temperature difference was found to be ~1.5 °C, using the chemical shift difference of $^{79}Br$ [42] with and without 20 msec of $^{1}H$ decoupling ($\omega/2\pi$ ~100 kHz, recycle delay of 2 sec), which is consistent with heating previously reported with a scroll coil in the bioMAS probe [43]. Data were processed with VnmrJ v3.1a (Agilent), NMRPipe [44], Gnuplot v4.6, and Sparky [45].

## 3. Results

### 3.1 Differential Scanning Calorimetry

To correlate the bilayer fluidity with the MAS solid-state NMR observables, we relied on membrane transporters from the SMR family [46, 47] reconstituted into synthetic lipid bilayers. The primary sequence and predicted transmembrane (TM) domains of the model SMR protein EmrE are shown schematically in Figure 1A. For carrying out the differential scanning calorimetry (DSC) experiments, we reconstituted EmrE into DMPC (14:0) and DPPC (16:0) liposomes at a lipid:protein ratio of 100:1. The lipid only vesicles were created

in an identical fashion through detergent to ensure similar liposome formation mediated by the polystyrene beads. The DSC thermogram data provides a plot of the heat capacity as a function of temperature with the peaks corresponding to phase transitions. In this work, we integrated the DSC data as a proxy for bilayer fluidity which is essentially the fraction of lipids in the liquid-crystalline phase [32]. All values of fluidity are reported as *fluid fraction* that resulted from cumulative integration of the main phase transition peak from the DSC thermogram data. In the gel phase, the bilayer is ordered and rigid (fluid fraction = 0), whereas in the liquid-crystalline phase, the bilayer is dynamic and disordered (fluid fraction = 1) [30, 32, 34]. Figure 2 shows the lipid-only bilayers where the pre-transition (gel to ripple phase transition) is seen as a small, broad peak at ~10 °C below the main phase transition for both DMPC and DPPC bilayers (Figure 2A and D). This phase transition is considered the start of bilayer melting, and is a period where the bilayer is dominated by rigid lipid acyl chains, periodically separated by more fluid lipid acyl chains, as well as marking the point where the fluid fraction begins to rise [34, 35]. In the absence of protein, the main phase transition ($T_m$) is highly cooperative, exhibiting a sharp and narrow peak. Identical DSC experiments were carried out in the presence of native EmrE, and show that the pre-transition in DMPC is no longer detectable and the main phase transition is significantly broadened (Figure 2B) as previously demonstrated for a wide variety of integral membrane proteins [37, 48, 49]. The effects on the $T_m$ are similar for DPPC in that the main phase transition is also broadened relative to the protein-free state (Figure 2E). However, unlike DMPC, the pre-transition in the presence of 100:1 lipid:EmrE remains visible in the DSC thermogram (Figure 2D). This result is consistent with previous experiments showing a negative correlation between pre-transition sensitivity to protein incorporation and lipid acyl chain length, possibly due to the hydrophobic mismatch in length between the protein and the lipid hydrocarbon chains [37].

### 3.2 Temperature Effects on $^{1}H$-$^{13}C$ Cross-polarization

To measure NMR lineshapes and signal intensities under different lipid phases, we recorded 1D $^{1}H$-$^{13}C$ cross-polarization (CP) spectra as a function of temperature in order to mimic the DSC experiments. Since all of our NMR experiments detected on $^{13}C$, we relied on a [$^{13}C_{\alpha}$,$^{15}N$-Leu] labeled EmrE sample in order to remove one-bond $^{13}C$-$^{13}C$ J-couplings that would otherwise increase linewidths and reduce spectral resolution. The protein was reconstituted into DMPC liposomes in an identical fashion as that used for the DSC experiments. Figure 3 shows the 1D $^{13}C$ CP spectra as a function of temperature, which reveals a dramatic sigmoidal dependence that begins with high signal intensities at frozen temperatures to reduced values at temperatures above the main phase transition. The latter effect has been described in the literature for solid-state NMR lineshapes and other biophysical methods [25, 29], and is a result of uniaxial rotational diffusion of membrane proteins in an intermediate timescale regime that induces a line-broadening effect [29]. From the Saffman-Delbrück equation [50] we estimated a rotational rate of ~$1.5 \times 10^5$ $s^{-1}$ at 25 °C, using a literature bilayer viscosity of 4 poise [51], and EmrE dimer dimensions of ~25 Å (height) and ~15 Å (radius) [52]. This rate is comparable to the frequencies of the NMR observables, resulting in the observed peak broadening. Unlike what was observed with the M2 transmembrane peptide [29], EmrE resonances did not become narrowed with increasing temperature, suggesting that the transporter remained in an intermediate

rotational motion regime up to 46 °C. The linear temperature dependence in the Saffman-Delbrück equation most likely prevents rotational diffusion from entering a fast-regime for EmrE, explaining why the $^{1}H$-$^{13}C$ CP signal does not increase at higher temperatures.

In Figure 4, we observed that the MAS signal intensities dramatically decreased at temperatures above ~13 °C. Since the main phase transition was ~23 °C as determined by DSC, this suggested that the fluidity of the membrane prior to a significant melting was sufficient to induce an influential effect on the NMR spectra. While the pre-transition for DMPC proteoliposomes was broad beyond detection at a 100:1 lipid:protein ratio, we anticipate that a similar degree of fluidity remained in the presence of EmrE that enabled greater protein rotational motion in this *pre-transition-like* region [34]. Consistent with this observation are previous studies on cytochrome C oxidase by EPR spectroscopy [26] and bacteriorhodopsin by EPR spectroscopy [6] and flash photolysis [51] that showed decreased rotational correlation times in DMPC liposomes between the pre-transition and the main phase transition.

To examine if our observable applied to other model membranes with different phase transition temperatures, we repeated the MAS experiments with EmrE in DPPC (16:0, $T_m$ = 41°C). Consistent with the DMPC preparations, we used identical conditions for the DPPC reconstitutions as those corresponding to the DSC samples. The DPPC 1D CP spectra are shown in Figure 4 and also showed a sigmoidal dependence. Note that the signal to noise curve for DPPC was right-shifted relative to DMPC (Figure 4; midpoint of ~32 °C), reflecting the fact that the uniaxial rotational motion was dependent on the membrane fluidity as measured by DSC (Figure 2). The drop in the signal intensity again did not directly correspond to the bilayer melting, but rather the inflection point was ~12 °C lower than the main phase transition. In order to directly compare the bilayer fluid fraction with the NMR signal intensities, we normalized the latter from a scale of 0 to 1 with the overlay shown in Figure 5. A comparison between the lipid fluid fraction and the signal intensity shows that a small amount of mobility in the bilayer is sufficient to reduce NMR signal intensities in CP spectra prior to the main phase transition temperature. In fact, both the DMPC and DPPC signal intensity curves are left-shifted with respect to the DSC integrated curves. When the fluid fraction of the bilayer approaches ~5% a dramatic decrease in signal intensity becomes apparent in the spectra. For the lipids we tested, the 5% fluidity corresponds to ~10–20 °C below the main phase transition of the lipid. These data support the conclusion that residual fluidity present prior to the main phase transition leads to uniaxial rotational diffusion that may stem from the mobility created in the ripple phase of DMPC and DPPC [6, 53, 54].

### 3.3 Validation with a Second Membrane Protein, SugE

To obtain additional evidence for a second membrane protein, we performed the same $^{1}H$-$^{13}C$ CP temperature titration using SugE, an SMR protein of the SUG sub-class [47]. The protein was [U-$^{13}C$,$^{15}N$] and reverse labeled with Ile and Leu and reconstituted into 3:1 DMPC:DMPG liposomes. DMPC and DMPG are both 14:0 saturated lipids and have the same main phase transition temperature. Similar to the EmrE signal intensity profiles as a function of temperature, SugE also showed a sigmoidal dependence. Note that

we integrated an identical region (50–61 ppm) of the spectrum in order to avoid errors associated with natural abundance lipid signals. Consistent to the value for EmrE, we found that at ~12 °C the intensity of peaks in SugE begin to substantially diminish. This suggests that the conditions used for optimizing membrane proteins in a particular model lipid bilayer may be preserved for other proteins.

Furthermore, to confirm that uniaxial rotation was responsible for the line broadening observed, we carried out a $^{1}H$-$^{15}N$ CP experiment at a slow spinning rate of 5 kHz that was not sufficiently fast to remove the side bands. When uniaxial rotation is slow, the $^{15}N$ chemical shift anisotropy is not fully averaged, which results in the ability to detect spinning sidebands [3, 55]. As seen in Figure 6C, we observed these sidebands at temperatures below the main phase transition. However, at temperatures above 24 °C (i.e., > $T_m$) the sidebands are no longer present, which is indicative of faster whole-body uniaxial rotational motion of SugE in the bilayer.

### 3.4 Multidimensional Experiments to Investigate the Linewidths

Although the 1D spectra allowed for quantification of signal to noise, it was difficult to accurately quantify individual peak linewidths from these experiments. For this reason, we also recorded heteronuclear $^{15}N$-$^{13}CA$ 2D heteronuclear correlation spectra (NCA) with EmrE in DMPC liposomes. These experiments utilize two CP elements: (1) $^{1}H$ to $^{15}N$ and (2) a selective transfer from $^{13}C_{\alpha}$ to $^{15}N$ [40]. Similar to the temperature dependence of the 1D $^{13}C$ CP spectra, the signal intensities in the double CP experiments also gave a sigmoidal dependence (Figure 7). However, the 2D spectra paint a clearer picture with respect to the linewidths of the resonances and the overall spectral resolution. While the signal to noise was among the highest at temperatures < 0 °C, the spectra were poorly resolved in the 2D NCA experiments, which was indicative of inhomogeneous line broadening [56]. Interestingly, the most resolved 2D spectrum was obtained at ~9 °C (Figure 7A), which correlated with the temperature value where the signal intensity started to decrease in the 1D $^{13}C$ CP spectra (Figure 4). This can be seen for L85, which has a $^{13}C$ linewidth of ~0.4 ppm at ~9 °C, where at lower temperatures, L85 was broader and more unresolved (Figure 7C). This observable suggests that the optimal temperature for membrane protein resolution in model DMPC bilayers corresponds to a critical fluidity of ~5% (Figure 7C). In fact, the optimal resolution for DPPC also corresponded with this critical level of fluidity at which the 1D $^{13}C$ CP curves diminished in signal to noise (Figure 4 and 7D). Interestingly, the pre-transition of DPPC in the presence of EmrE was sufficient to introduce a large amount of uniaxial rotational motion and thus the optimal resolution was obtained at 24 °C (corresponding to 5% fluidity), which is ~8 °C lower than the pre-transition value. After the temperature exceeds the value corresponding to the 5% fluid fraction (*critical fluidity*) the rotational diffusion becomes exceedingly fast and becomes a line-broadening mechanism that interferes with the MAS averaging and results in intermediate exchange.

## 4. Discussion

The ability to study membrane proteins in lipid bilayers is the preferable way to obtain information about structure and dynamics. In pursuit of this objective, our results highlight a delicate balance between signal intensity and spectral resolution that is directly related to the

physical state of the lipid bilayers. In model membranes containing no protein, the disorder or fluidity of the bilayer slowly increases at the pre-transition, followed by a rapid increase in fluidity at the main phase transition (Figure 2C and 2F) [34]. However, in the presence of protein, the phase transitions are substantially broadened. A comparison of the lipid fluidity curves from DSC with our intensity retention (Figure 5) reveals a marked leftward temperature shift in the $^{1}H$-$^{13}C$ CP plot, suggesting the presence of sufficient membrane fluidity prior to the main phase transition [37]. Specifically, the DSC/solid-state NMR correlation plots suggest that the most important temperature for optimal solid-state NMR spectra corresponds to a ~5% fluidity, where 5% of the lipids are in the fluid-fraction, as measured by DSC. In other words, for the solid-state NMR spectra, this temperature value acts as a fulcrum point of *critical fluidity*. At this temperature, the uniaxial rotational motion is slow enough to not dramatically interfere with the NMR observables, resulting in optimal linewidths and only marginal 10–20% losses in signal to noise relative to the frozen samples. In fact, the spectra acquired at this critical fluidity were devoid of severe inhomogeneous line broadening present in spectra acquired below 0 °C [56]. Since MAS studies of helical membrane proteins suffer primarily from resolution due to the similarity of chemical shifts, it is essential to optimize the experimental conditions that give the best resolution. We found that when the bilayer fluidity exceeds ~5–10%, the resulting spectra are substantially worse in both sensitivity and resolution as a result of the protein's uniaxial rotational motion moving from the slow to intermediate chemical exchange regime. This finding is pertinent to the rotationally aligned method that requires fast uniaxial rotational motion to calculate anisotropic NMR parameters with respect to the membrane normal (e.g., tilt angles) without preparation of a macroscopically aligned sample [25, 29, 33].

Our conclusions are based on data obtained from two membrane proteins (EmrE and SugE) and are consistent with common temperatures employed for other membrane proteins that have given high-quality spectra in the literature [2, 33]. For EmrE and SugE, we were unable to obtain a temperature regime that corresponded to fast uniaxial motion relative to the chemical shift frequencies. In other words, a fully fluid bilayer gave membrane protein spectra that were severely broadened. Based on the rotational diffusion rate calculated from the Saffman-Delbrück equation for the EmrE dimer (8 TM domains), we anticipate a similar result for other large polytopic membrane proteins, where temperatures above the main phase transition of synthetic lipid bilayers will be insufficient to enter the fast uniaxial rotational regime with respect to the NMR observables (chemical shift anisotropy and dipolar couplings). This represents a challenge for studying large polytopic membrane proteins in model membranes and necessitates the study of these samples in conditions that limit the rotational diffusion. A possible alternative to overcoming the limitations of studying membrane proteins above the main phase transition is to decrease the lipid to protein molar ratio. For example, our experimental conditions utilized a 170:1 lipid:dimer molar ratio, which would give ~3 lipid hydration layers surrounding the EmrE dimer on each leaflet (assuming a PC headgroup area of 0.65 $nm^2$ [57] and an EmrE dimer radius of 15 Å). From this calculation, this would give ~4 layers of unbound lipids between the EmrE dimer and the boundary lipid layer. Therefore, removal of unbound lipids by reducing the lipid to protein ratio may result in a membrane with effectively greater viscosity and a

decreased rotational diffusion rate of the protein under conditions above the nominal protein-lipid phase transition.

Future studies on polytopic membrane proteins will benefit from the use of lipid extracts or lipid compositions that closely mimic the biological membrane. Indeed, one potential drawback of model liposomes is that the chain length of the synthetic lipids can influence protein tilt angles and function due to effects arising from hydrophobic mismatch [29, 58, 59]. In addition, from a biological perspective, native membranes are believed to be more mosaic and viscous than the fluid conditions used for many biophysical studies of model membranes [60]. Indeed, it has been shown that using a eukaryotic membrane mimic containing cholesterol that the M2 transmembrane peptide showed significantly slower rotational diffusion compared to measurements in model DMPC bilayers [61]. Thus, the use of biological membrane mimics are likely to provide an avenue to studying polytopic membrane proteins at physiological temperatures that also enable high-quality NMR spectra to be obtained [62, 63].

## 5. Concluding Remarks

We carried out a comparative DSC/solid-state NMR study and observed that a critical fluidity of ~5% gave optimal spectral resolution while maintaining acceptable sensitivity for carrying out structural studies of membrane proteins in model lipid bilayers. These findings provide a framework for understanding the role of temperature in balancing sensitivity and resolution in solid-state NMR studies of polytopic membrane proteins in model lipid bilayers. In addition, our results suggest that DSC may provide a cost-effective route for screening lipid conditions for studying non-crystalline proteoliposome samples by MAS solid-state NMR spectroscopy.

## Acknowledgments

This work was supported by NIH grant K22AI083745 and start-up funds from New York University (to N.J.T.). J.R.B. acknowledges support from the Margaret-Strauss Kramer Fellowship. The authors acknowledge Prof. Jin Montclare for use of the DSC instrument.

## ABBREVIATIONS

| | |
|---|---|
| **SSNMR** | Solid-state NMR |
| **MAS** | magic-angle-spinning |
| **CP** | cross-polarization |
| **DSC** | differential scanning calorimetry |
| **DMPC** | 1,2-dimyristoyl-*sn*-glycero-3-phosphocholine |
| **DPPC** | 1,2-dipalmitoyl-*sn*-glycero-3-phosphocholine |

## References


1. Gayen A, Banigan JR, Traaseth NJ. Ligand-Induced Conformational Changes of the Multidrug Resistance Transporter EmrE Probed by Oriented Solid-State NMR Spectroscopy. Angewandte Chemie International Edition. 2013; 52:10321–10324.
2. Good DB, Wang S, Ward ME, Struppe J, Brown LS, Lewandowski JR, Ladizhansky V. Conformational Dynamics of a Seven Transmembrane Helical Protein Anabaena Sensory Rhodopsin Probed by Solid-State NMR. Journal of the American Chemical Society. 2014
3. Das BB, Nothnagel HJ, Lu GJ, Son WS, Tian Y, Marassi FM, Opella SJ. Structure Determination of a Membrane Protein in Proteoliposomes. Journal of the American Chemical Society. 2012; 134:2047–2056. [PubMed: 22217388]
4. Ghimire H, Abu-Baker S, Sahu ID, Zhou A, Mayo DJ, Lee RT, Lorigan GA. Probing the helical tilt and dynamic properties of membrane-bound phospholamban in magnetically aligned bicelles using electron paramagnetic resonance spectroscopy. Biochimica et Biophysica Acta (BBA) - Biomembranes. 2012; 1818:645–650.
5. Tiburu EK, Gulla SV, Tiburu M, Janero DR, Budil DE, Makriyannis A. Dynamic Conformational Responses of a Human Cannabinoid Receptor-1 Helix Domain to Its Membrane Environment. Biochemistry. 2009; 48:4895–4904. [PubMed: 19485422]
6. Davoust J, Bienvenue A, Fellmann P, Devaux PF. Boundary lipids and protein mobility in rhodopsin-phosphatidylcholine vesicles. Effect of lipid phase transitions. Biochimica et Biophysica Acta (BBA) - Biomembranes. 1980; 596:28–42.
7. McDermott A. Structure and Dynamics of Membrane Proteins by Magic Angle Spinning Solid-State NMR. Annual Review of Biophysics. 2009; 38:385–403.
8. Tycko R. Solid-State NMR Studies of Amyloid Fibril Structure. Annual Review of Physical Chemistry. 2011; 62:279–299.
9. Comellas G, Rienstra CM. Protein Structure Determination by Magic-Angle Spinning Solid-State NMR, and Insights into the Formation, Structure, and Stability of Amyloid Fibrils. Annual Review of Biophysics. 2013; 42:515–536.
10. Yan S, Suiter CL, Hou G, Zhang H, Polenova T. Probing Structure and Dynamics of Protein Assemblies by Magic Angle Spinning NMR Spectroscopy. Accounts of Chemical Research. 2013; 46:2047–2058. [PubMed: 23402263]
11. Opella SJ. Structure Determination of Membrane Proteins by Nuclear Magnetic Resonance Spectroscopy. Annual Review of Analytical Chemistry. 2013; 6:305–328.
12. Gopinath T, Mote KR, Veglia G. Sensitivity and resolution enhancement of oriented solid-state NMR: Application to membrane proteins. Progress in Nuclear Magnetic Resonance Spectroscopy. 2013; 75:50–68. [PubMed: 24160761]
13. Murray DT, Das N, Cross TA. Solid State NMR Strategy for Characterizing Native Membrane Protein Structures. Accounts of Chemical Research. 2013; 46:2172–2181. [PubMed: 23470103]
14. Lu G, Opella S. Resonance assignments of a membrane protein in phospholipid bilayers by combining multiple strategies of oriented sample solid-state NMR. Journal of biomolecular NMR. 2014; 58:69–81. [PubMed: 24356892]
15. Verardi R, Shi L, Traaseth NJ, Walsh N, Veglia G. Structural topology of phospholamban pentamer in lipid bilayers by a hybrid solution and solid-state NMR method. Proceedings of the National Academy of Sciences. 2011; 108:9101–9106.
16. De Angelis AA, Howell SC, Nevzorov AA, Opella SJ. Structure Determination of a Membrane Protein with Two Trans-membrane Helices in Aligned Phospholipid Bicelles by Solid-State NMR Spectroscopy. Journal of the American Chemical Society. 2006; 128:12256–12267. [PubMed: 16967977]
17. Knox RW, Lu GJ, Opella SJ, Nevzorov AA. A Resonance Assignment Method for Oriented-Sample Solid-State NMR of Proteins. Journal of the American Chemical Society. 2010; 132:8255–8257. [PubMed: 20509649]
18. Dürr UHN, Yamamoto K, Im SC, Waskell L, Ramamoorthy A. Solid-State NMR Reveals Structural and Dynamical Properties of a Membrane-Anchored Electron-Carrier Protein,

Cytochrome b5. Journal of the American Chemical Society. 2007; 129:6670–6671. [PubMed: 17488074]

19. Sharma M, Yi M, Dong H, Qin H, Peterson E, Busath DD, Zhou HX, Cross TA. Insight into the Mechanism of the Influenza A Proton Channel from a Structure in a Lipid Bilayer. Science. 2010; 330:509–512. [PubMed: 20966252]
20. Mahalakshmi R, Marassi FM. Orientation of the Escherichia coli Outer Membrane Protein OmpX in Phospholipid Bilayer Membranes Determined by Solid-State NMR†. Biochemistry. 2008; 47:6531–6538. [PubMed: 18512961]
21. Nevzorov AA. Orientational and Motional Narrowing of Solid-State NMR Lineshapes of Uniaxially Aligned Membrane Proteins. The Journal of Physical Chemistry B. 2011; 115:15406–15414. [PubMed: 22073926]
22. Traaseth NJ, Shi L, Verardi R, Mullen DG, Barany G, Veglia G. Structure and topology of monomeric phospholamban in lipid membranes determined by a hybrid solution and solid-state NMR approach. Proceedings of the National Academy of Sciences. 2009; 106:10165–10170.
23. Banigan JR, Traaseth NJ. Utilizing Afterglow Magnetization from Cross-Polarization Magic-Angle-Spinning Solid-State NMR Spectroscopy to Obtain Simultaneous Heteronuclear Multidimensional Spectra. The Journal of Physical Chemistry B. 2012; 116:7138–7144. [PubMed: 22582831]
24. Banigan JR, Gayen A, Traaseth NJ. Combination of (15)N reverse labeling and afterglow spectroscopy for assigning membrane protein spectra by magic-angle-spinning solid-state NMR: application to the multidrug resistance protein EmrE. Journal of biomolecular NMR. 2013; 55:391–399. [PubMed: 23539118]
25. Lewis BA, Harbison GS, Herzfeld J, Griffin RG. NMR structural analysis of a membrane protein: bacteriorhodopsin peptide backbone orientation and motion. Biochemistry. 1985; 24:4671–4679. [PubMed: 4063350]
26. Fajer P, Knowles PF, Marsh D. Rotational motion of yeast cytochrome oxidase in phosphatidylcholine complexes studied by saturation-transfer electron spin resonance. Biochemistry. 1989; 28:5634–5643. [PubMed: 2550057]
27. Smirnov AI, Smirnova TI, Morse PD 2nd. Very high frequency electron paramagnetic resonance of 2,2,6,6-tetramethyl-1-piperidinyloxy in 1,2-dipalmitoyl-sn-glycero-3-phosphatidylcholine liposomes: partitioning and molecular dynamics. Biophysical Journal. 1995; 68:2350–2360. [PubMed: 7647239]
28. Bonev BB, Chan WC, Bycroft BW, Roberts GCK, Watts A. Interaction of the Lantibiotic Nisin with Mixed Lipid Bilayers: A 31P and 2H NMR Study. Biochemistry. 2000; 39:11425–11433. [PubMed: 10985788]
29. Cady SD, Goodman C, Tatko CD, DeGrado WF, Hong M. Determining the Orientation of Uniaxially Rotating Membrane Proteins Using Unoriented Samples: A 2H, 13C, and 15N Solid-State NMR Investigation of the Dynamics and Orientation of a Transmembrane Helical Bundle. Journal of the American Chemical Society. 2007; 129:5719–5729. [PubMed: 17417850]
30. Janiak MJ, Small DM, Shipley GG. Nature of the thermal pretransition of synthetic phospholipids: dimyristoyl- and dipalmitoyllecithin. Biochemistry. 1976; 15:4575–4580. [PubMed: 974077]
31. Wack DC, Webb WW. Synchrotron X-ray study of the modulated lamellar phase Pβ′ in the lecithin–water system. Physical Review A. 1989; 40:2712–2730. [PubMed: 9902459]
32. Heimburg T. Mechanical aspects of membrane thermodynamics. Estimation of the mechanical properties of lipid membranes close to the chain melting transition from calorimetry. Biochimica et Biophysica Acta (BBA) - Biomembranes. 1998; 1415:147–162.
33. Opella SJ. Structure Determination of Membrane Proteins in Their Native Phospholipid Bilayer Environment by Rotationally Aligned Solid-State NMR Spectroscopy. Accounts of Chemical Research. 2013; 46:2145–2153. [PubMed: 23829871]
34. Riske KA, Barroso RP, Vequi-Suplicy CC, Germano R, Henriques VB, Lamy MT. Lipid bilayer pre-transition as the beginning of the melting process. Biochimica et Biophysica Acta (BBA) - Biomembranes. 2009; 1788:954–963.
35. Heimburg T. A Model for the Lipid Pretransition: Coupling of Ripple Formation with the Chain-Melting Transition. Biophysical Journal. 2000; 78:1154–1165. [PubMed: 10692305]

36. Gomez-Fernandez JC, Goni FM, Bach D, Restall CJ, Chapman D. Protein-lipid interaction: Biophysical studies of (Ca2+ + Mg2+)-ATPase reconstituted systems. Biochimica et Biophysica Acta (BBA) - Biomembranes. 1980; 598:502–516.
37. Zhang YP, Lewis RNAH, Hodges RS, McElhaney RN. Interaction of a peptide model of a hydrophobic transmembrane .alpha.-helical segment of a membrane protein with phosphatidylcholine bilayers: Differential scanning calorimetric and FTIR spectroscopic studies. Biochemistry. 1992; 31:11579–11588. [PubMed: 1445893]
38. Prenner EJ, Lewis RNAH, Kondejewski LH, Hodges RS, McElhaney RN. Differential scanning calorimetric study of the effect of the antimicrobial peptide gramicidin S on the thermotropic phase behavior of phosphatidylcholine, phosphatidylethanolamine and phosphatidylglycerol lipid bilayer membranes. Biochimica et Biophysica Acta (BBA) - Biomembranes. 1999; 1417:211–223.
39. Bennett AE, Rienstra CM, Auger M, Lakshmi KV, Griffin RG. Heteronuclear decoupling in rotating solids. The Journal of Chemical Physics. 1995; 103:6951–6958.
40. Baldus M, Petkova AT, Herzfeld J, Griffin RG. Cross polarization in the tilted frame: assignment and spectral simplification in heteronuclear spin systems. Molecular Physics. 1998; 95:1197–1207.
41. Ammann C, Meier P, Merbach A. A simple multinuclear NMR thermometer. Journal of Magnetic Resonance (1969). 1982; 46:319–321.
42. Thurber KR, Tycko R. Measurement of sample temperatures under magic-angle spinning from the chemical shift and spin-lattice relaxation rate of 79Br in KBr powder. Journal of Magnetic Resonance. 2009; 196:84–87. [PubMed: 18930418]
43. Stringer JA, Bronnimann CE, Mullen CG, Zhou DH, Stellfox SA, Li Y, Williams EH, Rienstra CM. Reduction of RF-induced sample heating with a scroll coil resonator structure for solid-state NMR probes. Journal of Magnetic Resonance. 2005; 173:40–48. [PubMed: 15705511]
44. Delaglio F, Grzesiek S, Vuister G, Zhu G, Pfeifer J, Bax A. NMRPipe: A multidimensional spectral processing system based on UNIX pipes. Journal of biomolecular NMR. 1995; 6:277–293. [PubMed: 8520220]
45. Goddard, TD.; Kneller, DG. Sparky 3. University of California; San Francisco: 2006.
46. Schuldiner S. EmrE, a model for studying evolution and mechanism of ion-coupled transporters. Biochimica et Biophysica Acta (BBA) - Proteins and Proteomics. 2009; 1794:748–762.
47. Bay DC, Rommens KL, Turner RJ. Small multidrug resistance proteins: A multidrug transporter family that continues to grow. Biochimica et Biophysica Acta (BBA) - Biomembranes. 2008; 1778:1814–1838.
48. McElhaney RN. Differential scanning calorimetric studies of lipid-protein interactions in model membrane systems. Biochimica et Biophysica Acta (BBA) - Reviews on Biomembranes. 1986; 864:361–421.
49. Heyn MP, Blume A, Rehorek M, Dencher NA. Calorimetric and fluorescence depolarization studies on the lipid phase transition of bacteriorhodopsin- dimyristoylphosphatidylcholine vesicles. Biochemistry. 1981; 20:7109–7115. [PubMed: 7317369]
50. Saffman PO, Delbruck M. Brownian motion in biological membranes. Proceedings of the National Academy of Sciences of the United States of America. 1975; 72:3111–3113. [PubMed: 1059096]
51. Cherry RJ, Godfrey RE. Anisotropic rotation of bacteriorhodopsin in lipid membranes. Comparison of theory with experiment. Biophysical Journal. 1981; 36:257–276. [PubMed: 7284552]
52. Fleishman SJ, Harrington SE, Enosh A, Halperin D, Tate CG, Ben-Tal N. Quasi-symmetry in the Cryo-EM Structure of EmrE Provides the Key to Modeling its Transmembrane Domain. Journal of Molecular Biology. 2006; 364:54–67. [PubMed: 17005200]
53. Blume, A. Dynamic Properties. In: Cevc, G., editor. Phospholipids Handbook. Marcel Dekker, Inc; New York: 1993. p. 467-484.
54. Mayer C, Mtiller K, Weisz K, Kothe G. Deuteron N.M.R. relaxation studies of phospholipid membranes. Liquid Crystals. 1988; 3:797–806.
55. Park SH, Das BB, De Angelis AA, Scrima M, Opella SJ. Mechanically, Magnetically, and “Rotationally Aligned” Membrane Proteins in Phospholipid Bilayers Give Equivalent Angular Constraints for NMR Structure Determination. The Journal of Physical Chemistry B. 2010; 114:13995–14003. [PubMed: 20961141]

56. Su Y, Hong M. Conformational Disorder of Membrane Peptides Investigated from Solid- State NMR Line Widths and Line Shapes. The Journal of Physical Chemistry B. 2011; 115:10758–10767. [PubMed: 21806038]

57. Dickey A, Faller R. Examining the Contributions of Lipid Shape and Headgroup Charge on Bilayer Behavior. Biophysical Journal. 2008; 95:2636–2646. [PubMed: 18515396]

58. Charalambous K, Miller D, Curnow P, Booth P. Lipid bilayer composition influences small multidrug transporters. BMC Biochemistry. 2008; 9:31. [PubMed: 19032749]

59. Lee AG. How lipids affect the activities of integral membrane proteins. Biochimica et Biophysica Acta (BBA) - Biomembranes. 2004; 1666:62–87.

60. Engelman DM. Membranes are more mosaic than fluid. Nature. 2005; 438:578–580. [PubMed: 16319876]

61. Weingarth M, Prokofyev A, van der Cruijsen EAW, Nand D, Bonvin AMJJ, Pongs O, Baldus M. Structural Determinants of Specific Lipid Binding to Potassium Channels. Journal of the American Chemical Society. 2013; 135:3983–3988. [PubMed: 23425320]

62. Luo W, Cady SD, Hong M. Immobilization of the Influenza A M2 Transmembrane Peptide in Virus Envelope–Mimetic Lipid Membranes: A Solid-State NMR Investigation. Biochemistry. 2009; 48:6361–6368. [PubMed: 19489611]

63. Gustavsson M, Traaseth NJ, Veglia G. Probing ground and excited states of phospholamban in model and native lipid membranes by magic angle spinning NMR spectroscopy. Biochimica et Biophysica Acta (BBA) - Biomembranes. 2012; 1818:146–153.

## Highlights

- NMR investigation of temperature effects for membrane proteins in lipid bilayers
- Solid-state NMR membrane protein spectra were correlated to lipid bilayer fluidity
- Optimal NMR spectral resolution was found ~15 °C below bilayer melting
- Broad MAS spectra persisted above bilayer melting temperature (intermediate regime)

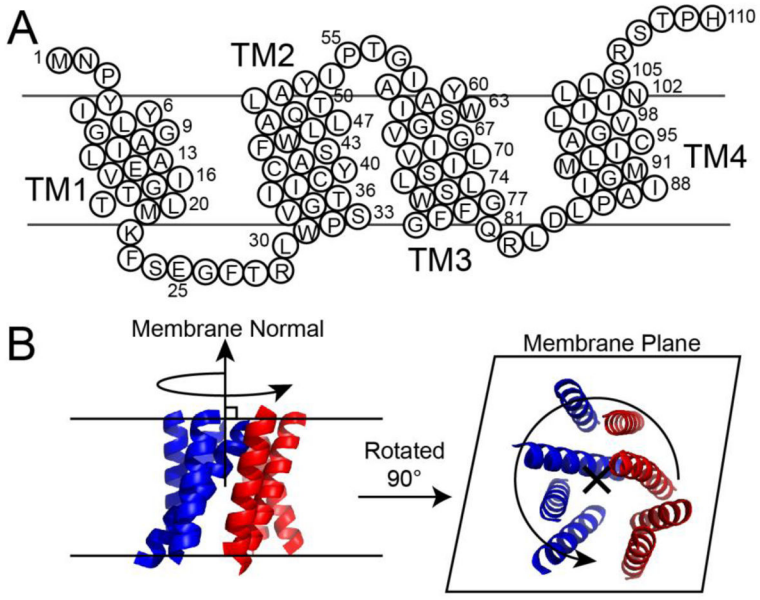


**Figure 1.**

(a) Sequence and transmembrane domains of the EmrE monomer. (b) Depiction of EmrE undergoing uniaxial rotation diffusion in the lipid bilayer, where the axis of rotation is parallel to the membrane normal. The image of EmrE is from PDB *2I68* [52].

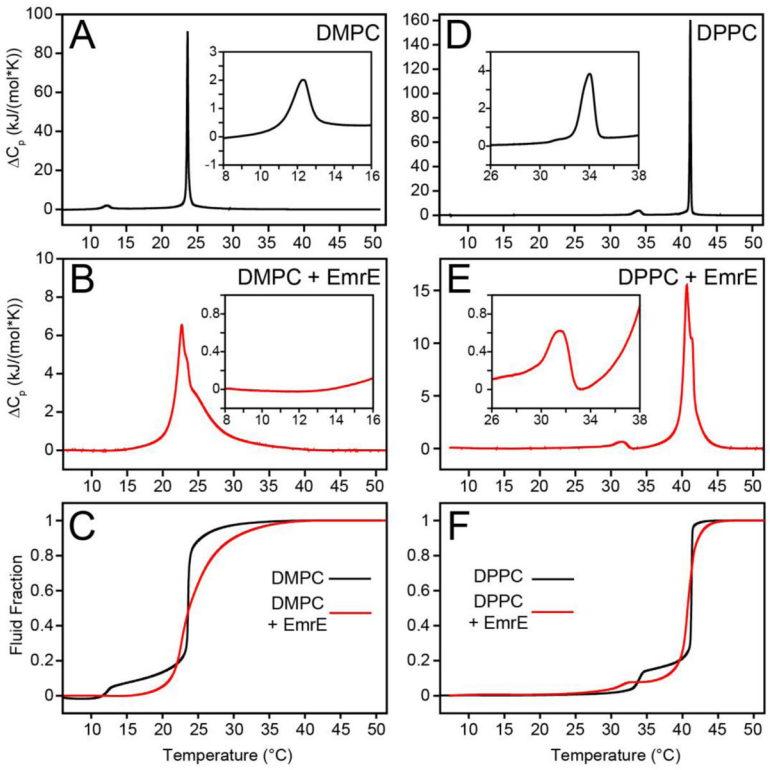


**Figure 2.**

Excess heat capacity was measured by DSC for (a) DMPC ($\Delta T_{m,1/2}$ = 0.19 °C) and (b) DMPC with EmrE ($\Delta T_{m,1/2}$ = 4.5 °C). In the presence of protein, the main phase transition is broadened and the pre-transition vanishes. (c) The fraction of lipids in a fluid-state, or liquid-crystalline phase, was determined by cumulative integration of $\Delta C_p$ followed by normalization with respect to the total enthalpy change. The same experiments were performed with (d) DPPC only ($\Delta T_{m,1/2}$ = 0.17 °C) and (e) DPPC with EmrE ($\Delta T_{m,1/2}$ = 1.4 °C). (f) The fluid fraction of DPPC. The insets in panels a, b, d, and e highlight the pre-transition region in each thermogram. The lipid concentration was 9.2 mM and the lipid:protein ratio was 100:1 (lipid:monomer), when protein was present.

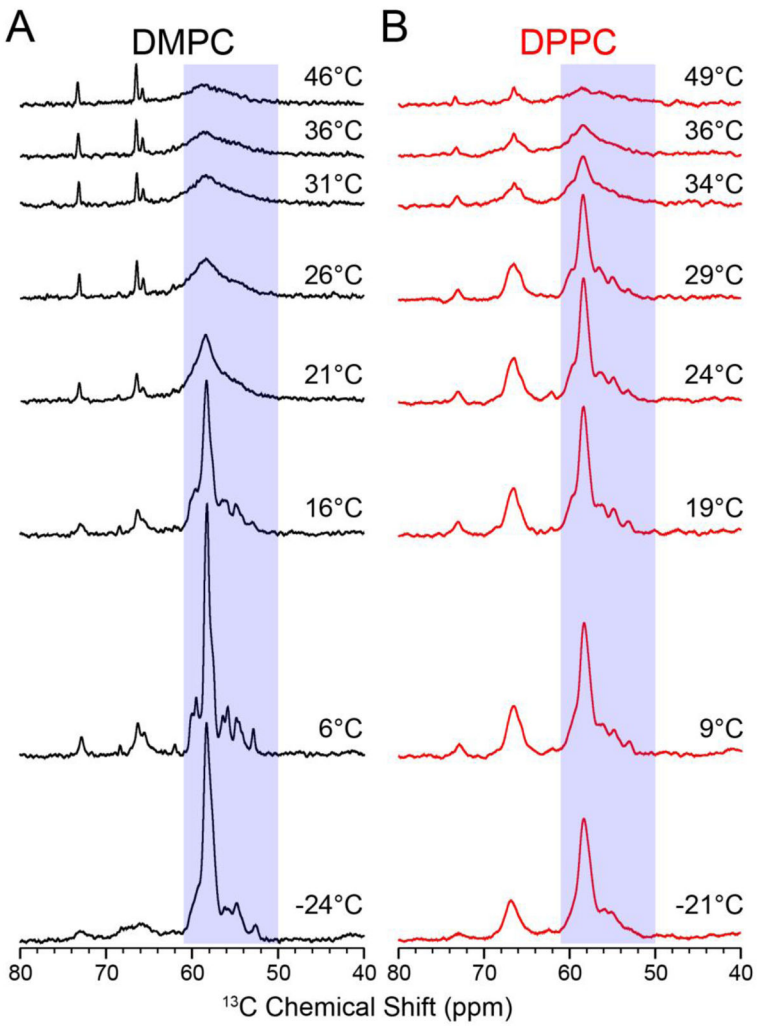


**Figure 3.**

1D $^{1}$H-$^{13}$C cross-polarization spectra of the temperature titration with EmrE in (a) DMPC and (b) DPPC. The boxes indicate the region used for intensity integration (50–61 ppm) shown in Figure 4. The main phase transition temperatures determined from the DSC data were 22.7 °C and 40.7 °C for DMPC and DPPC proteoliposomes, respectively. As the temperature increases, the NMR signal becomes broader due to increased uniaxial rotation. At the value of *critical membrane fluidity* (corresponding to ~5%), the signal intensity drops rapidly as the protein's uniaxial rotation enters the intermediate motional regime.

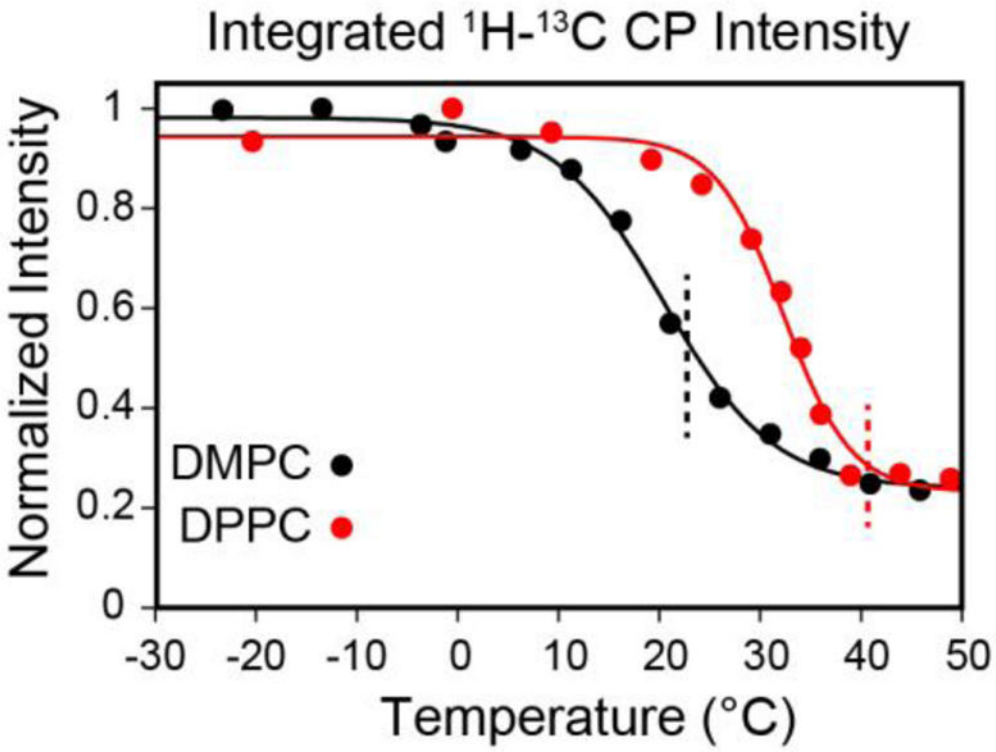


**Figure 4.**

The integrated signal intensities for [$^{13}$Cα,$^{15}$N-Leu] EmrE in DMPC (black) and [$^{13}$C,$^{15}$N-Val, $^{13}$Cα,$^{15}$N-Leu] EmrE in DPPC (red) from the spectra in Figure 3. The integrations were carried out between 50 and 61 ppm in the $^{13}$C spectra. The solid curves represent sigmoidal fits for the two lipid compositions, where the inflection point is at 20.4 °C for DMPC and 32.3 °C for DPPC. The dashed lines mark $T_m$ for DMPC (black, 22.7 °C) and DPPC (red, 40.7 °C).

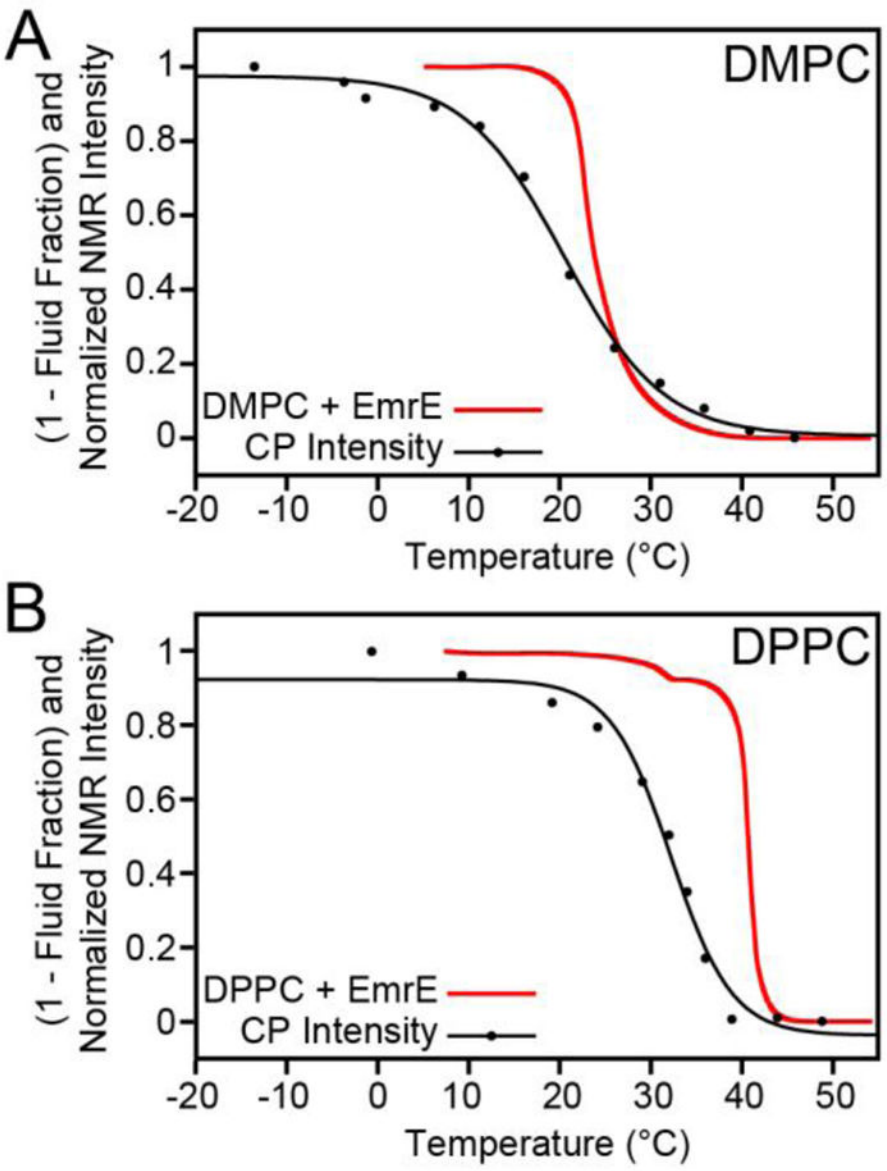


**Figure 5.**

Comparison of the DSC relative bilayer fluidity with the NMR signal intensities. The fluid fraction was determined from DSC by integrating $\Delta C_p$ and normalizing it to the enthalpy corresponding to bilayer melting ($T_m$). Note that this is plotted as (1 – fluid fraction) and is inverted relative to Figure 2C and 2F, for easier comparison with the NMR signal intensities. The NMR signal intensities from Figure 4 were renormalized from 0 to 1 in order to directly compare with the DSC data. The NMR data acquired in DMPC (panel a) and DPPC (panel b) both show sharp drops in signal intensity prior to bilayer melting, which shows that there is sufficient motion to allow intermediate uniaxial rotational diffusion that leads to signal line broadening.

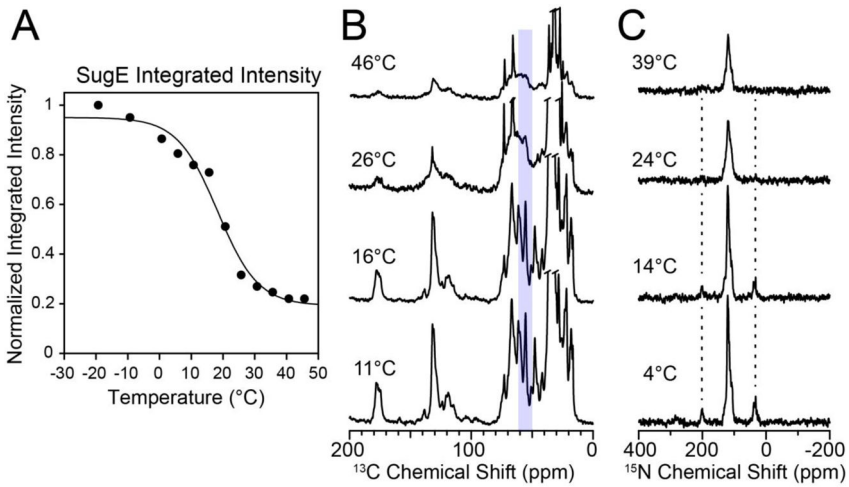


**Figure 6.**

MAS CP spectra and normalized intensities for the membrane transporter SugE in lipid bilayers. (A) Normalized intensity versus temperature of reverse-Ile/Leu labeled SugE in 3:1 DMPC/DMPG proteoliposomes. The black line is a sigmoidal fit of the normalized integrated intensity (the inflection point is at 18.3 °C). The intensities were obtained by integrating the $^{13}C$ spectra between 50 and 61 ppm. (B) 1D $^{1}H$-$^{13}C$ CP spectra of SugE that were integrated in panel A. (C) 1D $^{1}H$-$^{15}N$ spectra of SugE at a spinning rate of 5 kHz. The spinning sidebands are visible at lower temperatures when the uniaxial rotational motion is slow and subsequently disappear as the membrane environment becomes more fluid at temperatures above the main phase transition.

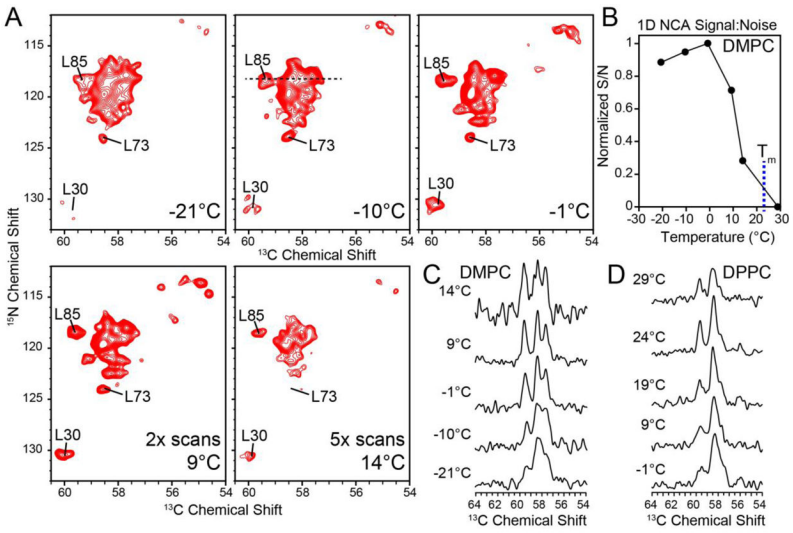


**Figure 7.**

(a) 2D NCA spectra of $TPP^+$-bound EmrE in DMPC as a function of temperature. The spectra at 9 °C and 14 °C were acquired with 2-fold and 5-fold the number of scans relative to the lower temperature spectra in order to account for the differences in signal-to-noise, respectively. (b) Normalized signal-to-noise (in 64 scans) versus temperature for the 1D N-CA with DMPC. The blue dashed line marks $T_m$ of DMPC. (c and d) Extracted 1D $^{13}C$ slices from the 2D NCA spectra ($^{15}N$ shift of 118.4 ppm) for DMPC and DPPC, respectively. The slices are shown at a normalized peak height. As the temperature increased above freezing, the linewidths improved, signal to noise and linewidth decrease upon crossing the point of critical fluidity. The optimal resolution occurs at a temperature when the signal:noise is less than the maximal value.